Biogeosciences Discuss., 11, 16269–16308, 2014
www.biogeosciences-discuss.net/11/16269/2014/
doi:10.5194/bgd-11-16269-2014

Biogeosciences Discussions
Open Access

Stable isotope paleoclimatology of the earliest Eocene using kimberlite-hosted mummified wood from the Canadian Subarctic

B. A. Hook[1], J. Halfar[2], Z. Gedalof[3], J. Bollmann[1], and D. Schulze[2]

[1]Department of Earth Sciences, University of Toronto, Toronto, ON M5S 3B1, Canada
[2]Department of Chemical and Physical Sciences, University of Toronto Mississauga, Mississauga, ON L5L 1C6, Canada
[3]Department of Geography, University of Guelph, Guelph, ON N1G 2W1, Canada

Received: 21 October 2014 – Accepted: 1 November 2014 – Published: 26 November 2014

Correspondence to: B. A. Hook (benjamin.hook@utoronto.ca)

Published by Copernicus Publications on behalf of the European Geosciences Union.

Abstract

The recent discovery of well-preserved mummified wood buried within a subarctic kimberlite diamond mine prompted a paleoclimatic study of the early Eocene "hothouse" (ca. 53.3 Ma). At the time of kimberlite eruption, the Subarctic and Artic were warm and humid producing a temperate rainforest biome well north of the Arctic Circle. Previous studies have estimated mean annual temperatures in this region were 4–20 °C in the early Eocene, using a variety of proxies including leaf margin analysis, and stable isotopes ($\delta^{18}O$) of fossil cellulose. Here, we examine stable isotopes of tree-ring cellulose at subannual to annual scale resolution, using the oldest viable cellulose found to date. We use mechanistic models and transfer functions to estimate earliest Eocene temperatures using mummified cellulose, which was well preserved in the kimberlite. Multiple samples of *Piceoxylon* wood within the kimberlite were crossdated by tree-ring width. Multiple proxies are used in combination to tease apart likely environmental factors influencing the tree physiology and growth in the unique extinct ecosystem of the Polar rainforest. Calculations of interannual variation in temperature over a multi-decadal time-slice in the early Eocene are presented, with a mean temperature estimate of 11.4 °C (1 σ = 1.8 °C) based on $\delta^{18}O$. Dual-isotope spectral analysis suggests that multidecadal climate cycles similar to the modern Pacific Decadal Oscillation likely drove temperature and cloudiness trends on 20–30 year timescales.

1 Introduction

1.1 Warm subarctic climates of the earliest Eocene

If anthropogenic fossil fuel burning continues unabated, pCO_2 levels are expected to reach 855–1130 ppmV by the end of the 21st century, leading to a 5.5 ± 0.6 °C temperature increase globally with nearly twice as much warming in Arctic regions (IPCC, 2013). In this "worst-case" climate change scenario, global temperatures will rapidly

BGD
11, 16269–16308, 2014

approach levels that have not existed on Earth for over 50 million years, since the Eocene. Greenhouse climates of the earliest Eocene were warm, with amplified warming at the poles (Greenwood and Wing, 1995), resulting from high atmospheric pCO_2 levels (~ 680–3300 ppmV) (Schubert and Jahren, 2013). Permanent polar ice caps did not exist; instead, vast temperate rainforests spanned the Arctic (Williams et al., 2003), and Antarctica (Francis, 1988; Francis and Poole, 2002; Ivany et al., 2011). The role that these forests played in Eocene climates is unknown, because such rainforests do not currently grow north of the Arctic Circle. Estimates of mean temperatures in the Eocene Arctic are much warmer than today, but they range widely, from 4–20 °C, based on a variety of proxies [e.g. leaf physiognomy (Greenwood and Wing, 1995; Sunderlin et al., 2011), bacterial membrane lipids (Weijers et al., 2007), oxygen isotope ratios in fossils of Eocene fauna (Fricke and Wing, 2004; Eberle et al., 2010), and oxygen isotopes of wood cellulose (Wolfe et al., 2012)]. Estimates of climate variability would benefit modeling efforts of greenhouse climates (Huber and Caballero, 2003) of past and future warm periods, but few studies have examined seasonal and interannual fluctuations from the early Eocene (Eberle et al., 2010).

Recently, wood megafossils were discovered in kimberlite diamond mines in the Northwest Territories of Canada (Wolfe et al., 2012). These wood specimens are not petrified, but mummified, many containing original woody material in a slightly altered state. A previous study found that thermal alteration of this wood was low (< 60 °C) (Hook et al., 2014). Preservation of the wood was aided by their inclusion in adiabatically chilled post-eruptive kimberlite backfill after eruption at ca. 53.3 Ma (Creaser et al., 2004). Samples of *Piceoxylon* Gothan 1905 wood from the Ekati Panda pipe owned by Dominion Diamond Corp. (64°42′49″ N, 110°37′10″ W) contain α-cellulose matching the Fourier Transform Infrared spectrum of modern cellulose standards (Hook et al., 2014). Therefore, we used these materials to investigate paleoclimates of the early Eocene, using a multi-proxy approach. By gathering records of annual tree-ring width and stable isotopes of $\delta^{13}C$ and $\delta^{18}O$ from the same tree rings, it is possible to glean more information than possible with a single proxy.

BGD
11, 16269–16308, 2014

1.2 Stable isotopes in paleoenvironmental research

The ratio of $\delta^{18}O$ in precipitation (i.e., source water – $\delta^{18}O_{sw}$) has a strong positive correlation with temperature in terrestrial systems outside of the tropics: Cooler (warmer) climates at higher latitudes and altitudes correspond with lower (higher) $\delta^{18}O_{sw}$. This has allowed construction of isotopic maps that depict average $\delta^{18}O_{sw}$ across geographic regions (Bowen, 2010; Bowen and Revenaugh, 2003). Precipitation $\delta^{18}O_{sw}$ is influenced by temperature, but also the location of evaporative sources, and continental rainout effects. Therefore, $\delta^{18}O_{sw}$ has been used to reconstruct past temperatures from hydrologically sensitive archives, such as tree rings, on an annual to subannual basis (DeNiro and Epstein, 1979; McCarroll and Loader, 2004; Roden et al., 2009).

After it was demonstrated that stable isotopes within tree rings could be used as an "isotopic thermometer" of past climates (Libby and Pandolfi, 1974; Libby et al., 1976), there has been a concerted effort to develop this proxy for the purposes of reconstructing temperatures before the modern instrumental period. Mechanistic models have been developed which predict the stable oxygen isotopic composition of α-cellulose ($\delta^{18}O_{cellulose}$) based on the isotopic ratio of source water ($\delta^{18}O_{sw}$) received by the tree (Flanagan et al., 1991; Roden et al., 2000; Anderson et al., 2002). These studies have found that in addition to $\delta^{18}O_{sw}$, factors that affect evaporative enrichment of leaf water (e.g., relative humidity – RH) also influence $\delta^{18}O_{cellulose}$. The problem with using mechanistic models in paleoenvironmental research is that many of these parameters (e.g., early Eocene RH, leaf temperature) are unknown. However, one may estimate a range of likely RH values and attain a range of likely temperature estimates based on the $\delta^{18}O_{cellulose}$ (Wolfe et al., 2012; Csank et al., 2013). Another approach is a transfer function, derived from plotting $\delta^{18}O_{cellulose}$ against $\delta^{18}O_{sw}$ from a number of samples and finding the best-fit relationship between them (Ballantyne et al., 2006; Richter et al., 2008b; Csank et al., 2013). Using this relationship, one may back-calculate an estimate of $\delta^{18}O_{sw}$ using $\delta^{18}O_{cellulose}$ of fossil cellulose. Temperature may then be estimated

BGD
11, 16269–16308, 2014

from $\delta^{18}O_{sw}$ using a $\delta^{18}O$-temperature relationship developed using isotope ratios of Eocene materials from different geographical locations (Fricke and Wing, 2004).

Other factors may have affected $\delta^{18}O_{sw}$ besides temperature. The modern temperature–$\delta^{18}O_{sw}$ relationship (Dansgaard, 1964) is different than in the Eocene because polar ice caps and glaciers are depleted in ^{18}O, and in the Eocene these ^{16}O-rich ice masses did not exist. Additionally, in the Eocene "equable" climate, latitudinal temperature gradients were not as steep as they are today, so condensation patterns may have been different (Greenwood and Wing, 1995; Fricke and O'Neil, 1999). Plant transpiration sends isotopically light oxygen into the atmosphere, which may be used by other plants, thus decreasing $\delta^{18}O_{cellulose}$ more than would be expected from temperature effects. The amount effect also lowers $\delta^{18}O_{sw}$ values through high levels of precipitation. In modern climate, this factor is more prevalent in tropical areas near the equator where heavy rainfall adds large amounts of ^{16}O, thus lowering the $\delta^{18}O_{sw}$ received by plants.

Trees receive CO_2 through stomatal apertures in the leaves. During C_3 photosynthesis, trees discriminate against CO_2 molecules containing ^{13}C resulting in a $\delta^{13}C$ depletion in plant matter relative to ambient air. However, this effect is altered in two scenarios which increase $\delta^{13}C$ in tree-ring records by reducing ^{13}C discrimination: (1) decreased relative humidity, leading to decreased stomatal aperture and decreased availability of ^{12}C molecules during carbohydrate fixation, and (2) increased photosynthetic rate as a result of increased sunlight availability. If a tree is growing in an arid region, hydrologic factors (e.g., vapor pressure deficit, relative humidity, precipitation) are more likely to dominate the $\delta^{13}C$ signal because stomatal controls over water loss also limit CO_2 intake, leading to higher $\delta^{13}C$ (Saurer et al., 1995; McCarroll and Loader, 2004). When the tree receives more solar radiation the photosynthetic rate increases, more CO_2 is required for glucose synthesis and ^{13}C discrimination is reduced, thus raising $\delta^{13}C$. Clouds limit solar radiation, causing a drop in $\delta^{13}C$, along with reduced C sequestration and photosynthetic assimilation (Alton, 2008). Therefore, records of

BGD
11, 16269–16308, 2014

$\delta^{13}C$ from *Pinus* trees growing near the Arctic Circle in Fennoscandia show strong correlations with cloudiness, allowing $\delta^{13}C$ from tree-ring cellulose to be used as a proxy for cloud cover (Young et al., 2010, 2012; Johnstone et al., 2013).

A common problem with studies of $\delta^{13}C$ in modern tree rings is related to the Suess effect, which describes the modern day $\delta^{13}C$ decline due to the addition of fossil fuel CO_2 to the atmosphere (McCarroll and Loader, 2004). Because fossil fuels are derived from plant matter, which discriminates against ^{13}C, the global average carbon isotope ratio ($\delta^{13}C_{atm}$) has dropped from a pre-industrial average of −6.4 ‰ to the modern average around −8 ‰ (McCarroll and Loader, 2004; McCarroll et al., 2009). In the early Eocene (ca. 53.3 Ma), $\delta^{13}C_{atm}$ was −5.7 ‰ based on isotopes of benthic foraminifera sampled from North Atlantic ocean sediments in locations where surface waters sink to the ocean floor and are well mixed by the thermohaline circulation (Tipple et al., 2010). Thus, $\delta^{13}C$ estimates from these benthic foraminifera record an archive of surface water productivity levels, which are influenced by $\delta^{13}C_{atm}$ (Zachos et al., 2001). Whereas $\delta^{13}C_{atm}$ varied on millennial timescales throughout the Cenozoic, it probably did not vary significantly throughout the life of the trees in this study.

Analysis of $\delta^{18}O$ and $\delta^{13}C$ measured simultaneously from tree-ring cellulose ("dual-isotope" analysis) may help constrain paleoclimatic signals better than a single isotopic ratio alone. As some environmental factors influence both $\delta^{18}O$ and $\delta^{13}C$ through stomatal controls, and other factors affect the isotopes independently, analyzing both isotopes together offers the possibility of teasing apart environmental factors. Conceptual models of dual-isotope behavior in tree rings in response to a range of environmental factors have been proposed (Scheidegger et al., 2000) and tested (Roden and Farquhar, 2012), with theorized relationships holding true in some cases. For example, factors affecting stomatal control influenced both $\delta^{18}O$ and $\delta^{13}C$. Changing RH and keeping all other variables fixed showed that $\delta^{18}O$ and $\delta^{13}C$ are indeed positively influenced by RH, leading to the positive correlation between $\delta^{18}O$ and $\delta^{13}C$ observed in trees growing in arid regions (Saurer et al., 1995, 1997). Low RH causes $\delta^{18}O$ to increase through evaporative loss of ^{16}O molecules (H_2O molecules are smaller than

BGD
11, 16269–16308, 2014

CO_2 molecules, hence stomata have a reduced effect compared to CO_2) (McCarroll and Loader, 2004). In water-stressed trees, leaf stomata have a strong control over the signals of both isotopes (Saurer et al., 1995); therefore dual-isotope series show a positive correlation with each other through time (Saurer et al., 1997; Liu et al., 2014). However, trees that grow in moist regions are typically not water-stressed, so other factors not related to stomata are more likely to be dominant. For instance, low light treatments affected $\delta^{13}C$ significantly, but not $\delta^{18}O$, indicating that $\delta^{13}C$ may be used as a proxy for past light levels (Roden and Farquhar, 2012). In practice, records of cloud cover in Fennoscandia match very closely to tree ring $\delta^{13}C$, leading to its use as a cloud cover proxy (Young et al., 2010, 2012).

In this study, we measured tree-ring width and stable isotopes ($\delta^{18}O$ and $\delta^{13}C$) at annual and subannual resolution from tree-ring cellulose extracted from multiple samples of *Piceoxylon* mummified wood. Our goal was to investigate seasonal, inter-annual, and possibly multidecadal variability in tree growth and physiological functioning in this unique ancient ecosystem. The extinct Polar Forest system is important to study, because it may allow improvements in vegetation boundary conditions in paleoclimate and future climate models, which are currently major sources of uncertainty (Huber and Caballero, 2011). For example, prodigious forest growth in the Subarctic and Arctic may have had profound implications in positive warming feedbacks, through changes in albedo and hydrologic regimes relative to today. Low albedo would have caused direct warming, while greater transpiration by trees would have increased water vapor in the Arctic atmosphere, which is a powerful greenhouse gas (Beerling and Franks, 2010; Jasechko et al., 2013). Therefore, Arctic temperature amplifications during equable climates may be partially explained by transpiration-related increases in water vapor.

BGD
11, 16269–16308, 2014

2 Methods

2.1 Sample materials and cellulose extraction

Samples of *Piceoxylon* wood from Ekati Panda kimberlite were surfaced, digitally scanned, and measured using a method developed specifically for mummified wood (Hook et al., 2013). Tree-ring series were crossdated using the skeleton plotting method (Stokes and Smiley, 1968), and the dendrochronology program library in R (dplR) (Bunn, 2008, 2010). A floating chronology of tree ring width indices (RWI) (six samples, time series $n = 92$) was created using a 100 year spline to remove the biological trend from the raw ring width series and strengthen the underlying climate signal. While RWI is a good parameter for general growth conditions, it responds to numerous climatic factors (e.g., temperature, precipitation, sunlight). Tree ring width data was compared with isotope data from the same tree rings using cross-correlation analysis to test whether $\delta^{18}O$ or $\delta^{13}C$ had any significant associations with RWI in the same, or lagged, tree rings (see Supplement for plot data).

We dissected individual tree rings into subannual samples (ranging from $n = 5$ to $n = 11$) to capture the climatic signal from wood formed during the growing season. Along with this seasonal study we dissected entire tree rings from wood transects for an annual-resolution study (three crossdated mummified wood samples, time series 86 year long). Kimberlite minerals were removed from the outer bark edge of samples and cross-sections (3 cm thick) were cut. Then transects were cut from the cross-sections from pith to bark, perpendicular to tree-ring boundaries. Transects were mechanically cleaned of kimberlite minerals, and then dissected into annual or sub-annual samples using a reflected-light microscope. Individual samples were placed in sterile glass vials and ground with a micro-pestle.

We used a Modified Brendel cellulose extraction method, a heated acid hydrolysis (via strong nitric/acetic acids) at 120 °C for 1 h to ensure complete delignification delignification (Brendel et al., 2000; Brookman and Whittaker, 2012). Following that, we used a 2.5 % NaOH to remove hemicelluloses, which have exchangeable oxygen

BGD
11, 16269–16308, 2014

atoms that may be replaced by ambient (modern) oxygen and bias the signal (Gaudinski et al., 2005; Richter et al., 2008a; Hook et al., 2014). Stable isotope ratios were measured at the Stable Isotope Laboratory at the University of Maryland. Cellulose was converted to carbon monoxide CO at 1080 °C over glassy carbon within a stream of 99.99 % He. Sample gas was then passed through traps for CO_2 and H_2O, and CO separated from N_2 by gas chromatography, before isotopic analysis on Continuous-Flow Micromass/Elementar Isoprime coupled to a Costech Analytical High Temperature Generator and Elemental Combustion System (Werner et al., 1996). Carbon and oxygen isotopic data were collected simultaneously from CO, corrected for runtime drift, amplitude dependence and scaling using widely separated working cellulose isotopic standards calibrated to international reference materials (Vienna Pee Dee Belemnite, VPDB for $\delta^{13}C$, and Standard Mean Ocean Water, SMOW, for $\delta^{18}O$). The overall precisions for the corrected data, based on replicate standard analyses, are 0.14 ‰ for $\delta^{13}C$ and 0.23 ‰ for $\delta^{18}O$.

2.2 Oxygen isotope analysis

To estimate early Eocene temperatures, the stable isotopic composition of $\delta^{18}O$ in tree ring cellulose ($\delta^{18}O_{cellulose}$) was used to estimate $\delta^{18}O$ of source water ($\delta^{18}O_{sw}$) using mechanistic models developed with modern plants (Roden et al., 2000). The Roden cellulose model uses a leaf-water $\delta^{18}O_{leaf}$ model to predict from $\delta^{18}O$ of source water (Flanagan et al., 1991) using Eq. (1):

$$\delta^{18}O_{wl} = \{(\alpha[\alpha_k \cdot R_{wx}(e_i - e_a/e_i) + R_{wa}(e_a/e_i)]/0.0020052) - 1\} \cdot 1000‰ \quad (1)$$

where R_{wx} and R_{wa} are the molar ratios of $^{18}O/^{16}O$ in leaf water, xylem water, and atmospheric water, respectively, α is the fractionation factor for liquid–vapor equilibrium of water, which depends on temperature (Majoube, 1971), α_k is the kinetic fractionation of water ($^{16}O/^{18}O = 1.0285$), and e_i and e_a are the partial pressures of water vapor in leaf intercellular spaces and in the atmosphere, respectively. Through a sensitivity

BGD
11, 16269–16308, 2014

analysis we found that the model was insensitive to changes in temperature, so we used optimal leaf temperature during photosynthesis (21.4 °C, Helliker and Richter, 2008) for calculation of α. Relative humidity (RH), however, had a large influence on the outcome, so we used a range of likely RH values in a temperate rainforest (64, 77, 83 %). The Roden et al. (2000) model uses the Flanagan et al. (1991) leaf-water model to predict $\delta^{18}O_{cellulose}$ following Eq. (2):

$$\delta^{18}O_{cellulose} = f_O \cdot (\delta^{18}O_{wx} + \varepsilon_O) + (1 - f_O) \cdot (\delta^{18}O_{wl} + \varepsilon_O) \quad (2)$$

Here f_O is the fraction of carbon-bound oxygen that is subject to isotopic exchange (42 %), $\delta^{18}O_{wx}$ is the isotope ratio of xylem water and ε_O is the biochemical fractionation factor related to conversion of sugar into cellulose (27 ‰). Xylem water is used as a close approximation to source water, which is valid because no fractionation occurs between soil water and the transference to xylem water (Barbour et al., 2002). Anderson et al. (2002) created a simplified model that combined the Flanagan et al. (1991) leaf-water model with the Roden et al. (2000) cellulose model, and reversed it to solve for $\delta^{18}O_{sw}$ using $\delta^{18}O_{cellulose}$ following Eq. (3):

$$\delta^{18}O_{sw} \approx \delta^{18}O_{cellulose} - (1 - f) \cdot (1 - h) + (\alpha + \alpha_k) - \varepsilon_{biochem} \quad (3)$$

Here f is a dampening factor related to isotopic fractionations between photosynthate and stem water and h is relative humidity. In addition to these mechanistic models, we used several transfer functions developed using modern tree-ring $\delta^{18}O_{cellulose}$ and its relationship to $\delta^{18}O_{sw}$ (Ballantyne et al., 2006; Richter et al., 2008b; Csank et al., 2013). A temperature–$\delta^{18}O_{sw}$ relationship developed for the Eocene was used to estimate the MAT based on $\delta^{18}O_{sw}$ (Fricke and Wing, 2004) (Table 1).

BGD
11, 16269–16308, 2014

2.3 Carbon isotope analysis

Isotopic discrimination against ^{13}C during photosynthesis has been modeled by Farquhar et al. (1982, 1989) following Eq. (4):

$$\Delta = a + (b - a)c_i/c_a \quad (4)$$

where Δ is the discrimination against ^{13}C, a is the fractionation due to diffusion through air (4.4 ‰), b is the fractionation due to carboxylation by RuBisCO (27 ‰), c_i and c_a are the partial pressures of CO_2 in the leaf intercellular spaces and atmosphere, respectively. To estimate $\delta^{13}C_{atm}$ from $\delta^{13}C_{cellulose}$ follow Eq. (5):

$$\delta^{13}C_{atm} = \delta^{13}C_{cellulose} + \Delta - \varepsilon_{pc} \quad (5)$$

where ε_{pc} is the average difference between bulk plant matter and cellulose. Cellulose is typically 2–5 ‰ higher (more enriched) than $\delta^{13}C$ of bulk plant tissue (ε_{pc} = 3.5 ‰ used in this study) (Barbour et al., 2002). The problem with this calculation is that Δ is dependent on the ratio of pCO_2 inside vs. outside the leaf (c_i/c_a), which is unknown for the Eocene. However, one may deduce c_i/c_a using the experimentally derived relationship between carbon isotope ratios of plant matter ($\delta^{13}C_p$) and the atmosphere ($\delta^{13}C_{atm}$) (Arens et al., 2000), and the cellulose isotopic offset from plant matter (ε_{pc} = 3.5 ‰), using Eq. (6):

$$\delta^{13}C_{atm} = (\delta^{13}C_{cellulose} + 18.72 - \varepsilon_{pc})/1.05 \quad (6)$$

To deduce c_i/c_a first one must solve for $\delta^{13}C_{atm}$ in Eq. (6), then for Δ in Eq. (5), and then for c_i/c_a in Eq. (4).

2.4 Dual-isotope analysis

Oxygen isotopes in cellulose are typically enriched by 20 to 30 ‰, whereas carbon isotopes are depleted (−20 to −25 ‰ range). Therefore, to make the isotopes more comparable, both datasets were normalized (mean = 0, variance = 1) and plotted together

BGD
11, 16269–16308, 2014

on one axis. The normalized isotope time series were then summed (subtracted) to amplify (suppress) isotopic variability common to both isotopes, and suppress (amplify) factors to which the isotopes do not respond in a similar manner. For instance, changes in stomatal conductance (e.g., due to changes in relative humidity or drought) affect both isotopes, so the dual-isotope time series should be positively correlated and vary in-phase with each other (Saurer et al., 1997). Any variance in the dual-isotope series that is not explained by this positive correlation is likely related to other factors. A factor that would likely influence $\delta^{13}C_{cellulose}$ (but not $\delta^{18}O_{cellulose}$) is a reduction in light, possibly by cloud coverage (Johnstone et al., 2013). On the other hand, $\delta^{18}O_{sw}$ would significantly affect $\delta^{18}O_{cellulose}$ (but not $\delta^{13}C_{cellulose}$) (Ferrio and Voltas, 2005).

One way to amplify an environmental signal common to two proxies is addition. Adding the normalized series together ($\Sigma_{Z\text{-score}}$) amplifies the in-phase components of the variance, and suppresses the out-of-phase components. Conversely, subtracting the dual-isotope series from each other ($\Delta_{Z\text{-score}}$) amplifies the out-of-phase components of the variance and suppresses the in-phase components. Principal Components Analysis (PCA) was conducted on the dual-isotope dataset to examine the variance structure. PCA on two variables produces a two-dimensional plot of two eigenvectors: PC1 and PC2, which are orthogonal to each other and identify factors that explain the most variance between the isotopes (PC1), as well as variance that is uncorrelated between the two datasets. Therefore, PC1 corresponds with $\Sigma_{Z\text{-score}}$, and PC2 with $\Delta_{Z\text{-score}}$, as described above. Spectral analysis was conducted (Multi-Taper Method, MTM, Mann and Lees, 1996; Singular Spectral Analysis, SSA, Vautard and Ghil, 1989; kSpectra software) on the raw data, PC1 ($\Sigma_{Z\text{-score}}$), and PC2 ($\Delta_{Z\text{-score}}$) time series to examine the temporal power spectra.

3 Results and discussion

Tree ring growth was prodigious in the earliest Eocene Subarctic (mean tree ring width for the *Piceoxylon* samples ranged from 1.88–2.19 mm, σ range = 0.65–0.76). How-

BGD
11, 16269–16308, 2014

ever, ring width series in this study were sensitive enough for crossdating (mean sensitivity values = 0.20–0.36). The overlapping ring sequences from the wood fragments were positively correlated, supporting the idea that the trees were subjected to similar climatic conditions (EPA3 vs. EPA4, $R = 0.38$, $p = 0.04$, $n = 30$). Some ring width series were so similar that they may have originated from the same tree (EPA4 vs. EPA6, $R = 0.90$, $p < 0.0001$, $n = 35$). Annual-resolution dual-isotope series were strongly correlated in both overlapping sections with regard to $\delta^{18}O$ (EPA3 vs. EPA4, $R = 0.78$, $p < 0.0001$, $n = 22$; EPA4 vs. EPA6, $R = 0.85$, $p < 0.0001$, $n = 31$) (lower two graphs in Fig. 1). One of the overlapping sections of $\delta^{13}C$ was strongly correlated (EPA3 vs. EPA4, $R = 0.73$, $p < 0.0001$, $n = 22$), but the other was strongly non-correlated (EPA4 vs. EPA6, $R = 0.01$, $p = 0.97$, $n = 31$). Both the RWI and $\delta^{18}O$ records correlate strongly in this section so it is unknown why $\delta^{13}C$ does not. Cross-correlation analysis of RWI and isotope series suggests that climatic conditions from the previous year or two significantly influence tree-ring width ($\delta^{18}O$ lagged −1 year before RWI, $R = 0.27$, $p = 0.02$, $n = 84$, $\delta^{18}O$ lagged −2 years before RWI, $R = 0.22$, $p = 0.04$, $n = 83$). Additionally, a positive correlation was found when $\delta^{18}C$ was lagged +2 with regard to RWI ($R = 0.23$, $p = 0.04$, $n = 83$). This correlation may indicate that increased tree-ring growth is associated with increased foliage production in the following years, thus leading to an increase in photosynthetic capacity and hence an increase in $\delta^{13}C$.

Days were long in the subarctic summer ($\sim 19\,h\ d^{-1}$ at summer solstace), allowing high rates of photosynthesis, provided solar radiation was not obscured by clouds. In the subannual study, the intra-annual series generally showed a rise and fall pattern throughout the growing season, suggesting that this wood is of a persistent-leaved species (upper two graphs in Fig. 1) (Barbour et al., 2001). Earlywood cellulose in deciduous species is isotopically enriched in $\delta^{13}C$ compared to persistent-leaves species, due to the use of carbohydrates stored in parenchyma over the dormant season (Jahren and Sternberg, 2008). Changes in relative humidity (RH) may be explained by a positive slope in a scatterplot of $\delta^{18}O$ and $\delta^{13}C$ (Roden and Farquhar, 2012). Theoretically, lowest RH (highest T) would be in midsummer when the continuous light

BGD
11, 16269–16308, 2014

regime is near its peak (Fig. 2). Other factors besides RH probably affected the isotope signals in most years not described by a simple rise and fall pattern along the RH slope however, as in tree ring (TR) 39 (Fig. 2). For instance, years with intense solar radiation could have raised the $\delta^{13}C$ without significantly altering $\delta^{18}O$. Traumatic resin ducts were observed in TR 40 and 42, and these rings showed an irregular scatterplot pattern (Fig. 2). Therefore, it is possible that disturbance (e.g., defoliation by insects) contributed to interruptions in these patterns. However, such disturbances are unlikely to substantially alter the climate signal on an annual basis, as modern trees do not show a strong isotopic response to disturbance from natural insect defoliation (Daux et al., 2011) or extreme experimental defoliation (Simard et al., 2012). Another factor in seasonal changes in $\delta^{13}C$ is an increase in $\delta^{13}C$ during peak growing season, when plants preferentially remove ^{12}C from the atmosphere (McCarroll and Loader, 2004).

The annual-resolution dual-isotope record was positively correlated (Pearson's R = 0.36, $P < 0.001$, n = 86) (Figs. 1 and 3). This suggests that stomatal conductance was an important factor in the physiological functioning of these trees (Saurer et al., 1995). However, the first 4–8 tree rings were noticeably lower in $\delta^{13}C$ than the rest of the tree rings, presumably due to a juvenile effect in which growth conditions are different (e.g., shadier) than mature trees. If these 4–8 rings are removed from analysis, the isotopes are no longer correlated (first four rings removed, Pearson's R = 0.17, P = 0.12, n = 82; first eight rings removed Pearson's R = 0.14, P = 0.22, n = 78). No correlation between the isotopes implies that stomatal conductance was less important than other climatic factors, suggesting that humid climates prevailed (Saurer et al., 1995). A previous study of middle Eocene (ca. 45 Ma) humidity found very high RH levels (80–100 %) by the end of the season using proxies derived from *Metasequoia* wood from high-Arctic Axel Heiberg Island (77° N paleolatitude) (Jahren and Sternberg, 2008). Using the $\delta^{18}O$ record, a range of temperature estimates was produced using the mechanistic models and transfer functions (Table 1). However, it is unknown which of these estimates is closest to actual Eocene temperatures. We estimated temperature based on different possible RH levels (64, 77, 83 %), as in Wolfe et al. (2012) and Csank et al. (2013), and

BGD
11, 16269–16308, 2014

then calculated mean, standard deviahtion (SD), 90 % confidence intervals, minimum and maximum of all models (Figs. 4 and 5).

Temperatures were generally warm according to this proxy record, staying above zero in the 90 % confidence interval; the range was 3.5–16.4 °C (n = 4), with a mean of 10.9 °C (1 σ = 3.0 °C) (black line in Fig. 4). Warm month mean temperatures (WMMT) would therefore be at the higher end of this growing season range (~ 16.4 ± 3.0 °C), which is in agreement with published records of high Arctic seasonal temperatures (19–20 °C, Eberle et al., 2010). Because tree-ring growth ceases during the winter, cold month mean temperatures (CMMT) cannot be directly calculated with this proxy. However, if independent estimates of CMMT based on Eocene MAT could be applied to our study. Estimates based on apatite of bowfin (*amiid*) fish that grow year-round suggest CMMT of 0–3.5 °C and an MAT of 8 °C (Eberle et al., 2010). In our annual study, the mean of all of the methods (black line in Fig. 5) ranged from 7.5–16.6 °C, with a mean of 11.4 °C (1 σ = 1.8 °C) (Table 2). This would suggest a CMMT of ~ 3.4–6.9 °C during the earliest Eocene based on the findings of Eberle et al. (2010) applied to our MAT estimate. The SD of all methods was 4.1 °C, and the 90 % confidence interval was 2.7 °C (Fig. 5). A mean temperature of 11.4 °C is close to other estimates of early Eocene MAT based on independent proxies (e.g., leaf margin analysis: 11–14 °C, Sunderlin et al., 2011). Some of the highest MAT estimates produced (> 20 °C) match estimates of warmest mean temperatures for the early Eocene (18–20 °C) (Weijers et al., 2007).

Our MAT estimate is 2.4 °C higher than that of Wolfe et al., (2012) (grand mean = 9 °C), but our mean estimate of 11.4 °C falls within the total range of MAT estimates provided by that study (7–12 °C). Their study was conducted on cellulose from *Metasequoia* trees from the same kimberlite mine (n = 4). However, bulk wood samples were taken in that study, precluding the possibility of examining climates from distinct years. We measured 141 individual tree rings from three crossdated tree-ring series spanning an 86 year-long period, and there were years in our record in which the MAT estimate was as low as 9 °C as in Wolfe et al. (2012). It may be that the cellulose sampled in that

BGD
11, 16269–16308, 2014

study grew during these years of slightly lower MAT, or that differences of 1–3 °C are not currently resolvable using these proxies and the values are essentially equivalent.

The carbon isotopic composition of the atmosphere ($\delta^{13}C_{atm}$) changes slowly over million year timescales (largely related to plate tectonic related forcing) (Zachos et al., 2001; Tipple et al., 2010). In the absence of a drastic event such as the Paleocene–Eocene Thermal Maximum this value is assumed to be constant over an average tree lifespan (< 1000 yr). In this study, mean $\delta^{13}C_{atm}$ was −5.3 ‰, based on mean $\delta^{13}C_{cellulose}$ (−20.8 ‰), using Eq. (6). Therefore, we assume any year-to-year changes in $\delta^{13}C_{cellulose}$ are related to changes in photosynthetic rate (A) and/or stomatal conductance (g_s). Compared to either the pre-industrial average (−6.4 ‰), or the modern average (−8 ‰), it is clear that the early Eocene atmosphere was enriched with respect to $\delta^{13}C$, in addition to having high atmospheric pCO_2 (c_a) (Royer, 2006; Schubert and Jahren, 2013). High c_a allows greater water use efficiency by plants because they do not have to open stomata as wide or as persistently to maintain adequate intercellular pCO_2 (c_i) for RuBisCO activity (McCarroll and Loader, 2004; Liu et al., 2007).

Experimental studies of modern plants find a positive relationship between c_i/c_a and pCO_2 in the atmosphere (Lomax et al., 2012). In the post-industrial period of pCO_2 addition to the atmosphere, a c_i/c_a of 0.45 in *Picea crassifolia* Kom. has decreased slightly in arid regions of China (Liu et al., 2007). However, greenhouse-grown seedlings c_i/c_a values were as high as 0.6 for *Picea glauca* (Moench) Voss. (Freeden and Sage, 1999) and 0.66 for *Picea abies* (L.) Karst (Wallin and Skärby, 1992). Using the estimated Eocene $\delta^{13}C_{atm}$ = −5.3 ‰, one may calculate Δ = 18.95 (Eq. 5), and c_i/c_a = 0.65 (Eq. 4). The similarity of this value to greenhouse-grown *Picea* seedlings (c_i/c_a = 0.6 to 0.66 range) suggests that the equable climates and high pCO_2 of the Eocene maintained relatively high c_i/c_a values (Wallin and Skärby, 1992; Freeden and Sage, 1999). The $\delta^{13}C_{atm}$ range given by c_i/c_a 0.6 to 0.66 range matches the 90 % confidence interval of $\delta^{13}C_{atm}$ by Tipple et al. (2010) for the early Eocene (mean $\delta^{13}C_{atm}$ = −5.7 ‰, 90 % confidence interval: −4.8 to −6.3 ‰) (Table 3).

BGD
11, 16269–16308, 2014

In the modern climate, the Suess effect greatly alters $\delta^{13}C_{atm}$, which is seen as a gradual downward curve starting with the industrial revolution, but in the Eocene $\delta^{13}C_{atm}$ levels were likely constant over the life of a tree. Therefore, any shifts upward or downward around the mean $\delta^{13}C_{cellulose}$ are likely related to changes in photosynthetic rate or stomatal conductance, both of which influence c_i/c_a. Therefore, we assume our $\delta^{13}C_{cellulose}$ record to be a qualitative proxy of sunlight/cloudiness, with the exception of a brief period during the juvenile phase of the tree's life. Growth conditions for trees in their juvenile years are slightly different than those of mature trees, because they must compete for light in the shaded understory, leading to a juvenile effect in the early part of some $\delta^{13}C$ records (Gagen et al., 2007).

Although precise quantitative estimates of sunlight cannot be made, analysis of both isotopes simultaneously can aid in qualitative assessment of solar variability. When both isotope datasets are normalized (Fig. 6, top graph) and summed (Fig. 6, middle graph), a signal related to RH and vapor pressure deficit (VPD) should be amplified, because both isotopes are affected by g_s (low RH, high VPD, causes an increase in both $\delta^{18}O_{cellulose}$ and $\delta^{13}C_{cellulose}$, leading to a positive correlation, Saurer et al., 1995). Conversely, when the dual isotope data are normalized and subtracted, the remaining unexplained variance relating to factors other than RH should be amplified (Fig. 6, bottom graph). For $\delta^{18}O_{cellulose}$, $\delta^{18}O_{sw}$ is a major factor (related to temperature of precipitation and precipitation sources), and for $\delta^{13}C_{cellulose}$ cloudiness is the most likely controlling factor because clouds limit photosynthetic rate. Modern trees growing near the Arctic Circle in Fennoscandia show high correlations between annual records of stable carbon isotope ratios ($\delta^{13}C$) and records of cloud cover, where the dominant factor in their $\delta^{13}C$ records is photosynthetic rate (Young et al., 2010, 2012). When more sunlight is received, photosynthetic rate is increased, which reduces isotopic discrimination and raises the $\delta^{13}C$ value. However, a converse relationship exists between sunlight and temperature at different timescales. Proxy records suggest that at high frequency timescales (annual), sunlight and temperature are positively related (i.e., sunny = warm, cloudy = cool), but at low frequencies (multidecadal), they are

BGD
11, 16269–16308, 2014

negatively related (i.e., cloudy = warm, sunny = cool) (Young et al., 2012). It is somewhat counterintuitive that sustained, regional warmer temperatures cause an increase in evaporation and cloud cover, bringing latent heat to northern latitudes through increased precipitation. Simultaneously, clouds cause short-term local cooling by blocking solar radiation.

Spectral analysis of the normalized summed data (PC1) shows a significant interannual-scale pattern (2–3 ypc) (Fig. 6, middle graph), whereas the normalized subtracted data (PC2) shows multidecadal cyclicity (20–30 ypc) (Fig. 6, bottom graph). This pattern is similar to modes of the modern Pacific Decadal Oscillation (PDO) and Arctic Oscillation/North Atlantic Oscillation (AO/NAO), which operate on multidecadal time-scales (Mantua et al., 1997; Young et al., 2012). These modes are also teleconnected with ENSO cycles (2–7 ypc) in the modern climate (Gershunov and Barnett, 1998). Temperature increases during positive phases of the PDO contribute to greater evaporation, leading to enhanced cloud formation and precipitation levels on a strongly bidecadal mode (Chiacchio et al., 2010). Sparse cloud cover may not significantly block sunlight, as diffusion may redistribute it through the canopy (Reinhardt et al., 2010; Urban et al., 2012). However, if cloud cover is very dense it may limit tree growth by blocking photons necessary for photosynthesis (Ritchie, 2010). Heavy cloud cover has been implicated in reduced photosynthetic rate of modern black spruce (*Picea mariana* (Mill.) Britton, Sterns & Poggenburg) growing at subarctic treeline in Quebec, Canada (Vowinckel et al., 1975).

When dual-isotope analyses (PC1, $\Sigma_{\text{Z-score}}$, and PC2, $\Delta_{\text{Z-score}}$) were compared with RWI data, an apparent positive association existed between PC2 and RWI at low frequencies. The middle portion (i.e., tree rings least likely affected by juvenile growth or diagenetic factors) of the 7 year running mean data was strongly positively correlated (TR 27–82; $R = 0.68$, $p < 0.0001$, $n = 55$) (Fig. 7). This suggests that PDO-like climate fluctuations of temperature and precipitation led to decades of increased tree growth during positive phases of the early Eocene "PDO", and decades of decreased growth during negative "PDO" phases. No association was found between PC1 and

BGD
11, 16269–16308, 2014

RWI records. If PC1 (positive correlation of isotopes) is related to Eocene RH, sustained high humidity may explain this non-association (i.e., low RH variability, Saurer et al., 1995).

In the early Eocene, subarctic trees may have been strongly dependent on both light and precipitation, and therefore influenced by cloud coverage. Sewall and Sloan (2001) hypothesized that in the Eocene, the lack of polar ice contributed to a stable positive Arctic Oscillation, rather than the multidecadal dipole that currently exists. However, the RWI and isotope data presented here suggest that PDO-like cyclicity operated in the early Eocene, possibly contributing to AO teleconnections as it does today (Jia et al., 2009). Oceanic Rossby waves may have set the timescale for multidecadal shifts in the position of the Aleutian low-pressure system, which changes the trajectory of weather patterns (Gershunov and Barnett, 1998). During positive PDO phases the position of the Aleutian low shifts southward, drawing in ENSO-mediated tropical moisture and delivering it to the Subarctic (Fig. 8). Another possibility for the $\delta^{18}O$ variation is multidecadal shifts in source water location (e.g., Pacific Ocean, Arctic Ocean). In the early Eocene the Arctic Ocean was isolated from other oceans, with high freshwater content from high precipitation (Brinkhuis et al., 2006). Thus, the Arctic Ocean source water would have been depleted in $\delta^{18}O$ relative to Pacific Ocean source water. Therefore, the trees in our study may have alternately received low-$\delta^{18}O$ from the Arctic, and high-$\delta^{18}O$ from the Pacific shifting every 20–30 years.

Jahren and Sternberg (2002) suggested that meridional transport of precipitation northward across the North American continent could have depleted the $\delta^{18}O$ of rainwater before reaching their study site. However, such a strong southerly wind current system seems unlikely in the Eocene, if the latitudinal temperature gradient was low (Greenwood and Wing, 1995), and given similar orbital variability (Laskar et al., 2011). However, if Eocene equatorial temperatures were high (35–40 °C, Caballero and Huber, 2010) temperature gradients may have been stronger than previously thought, leading to strong winds. Another possible explanation for the low $\delta^{18}O$ values of extreme northern polar forests in that study is that the source water was largely recycled

BGD
11, 16269–16308, 2014

from depleted Arctic Ocean sources, or water transpired from trees (Jasechko et al., 2013). Additionally, mineral contamination (e.g., by iron oxides) may also cause negative $\delta^{18}O$ errors (Richter et al., 2008a). Paleoclimate models suggest that increases in atmospheric water vapor due to an ice-free Arctic may have created conditions conducive to formation of a stable Arctic cyclone, through which southern precipitation sources could not penetrate (Sewall and Sloan, 2001). Our results suggest that if this stable Arctic cyclone existed then it probably still had teleconnections with a PDO-like mechanism, causing the edge of the cyclone to shift northward and southward on multidecadal timescales.

4 Conclusions

Multiple tree-ring based proxies were examined to study the climate of the early Eocene. The material used was extremely well preserved *Piceoxylon* Gothan 1905 mummified wood found in kimberlite diamond mines (ca. 53.3 Ma), which allowed geochemical investigations of primordial cellulose. Stable isotope data ($\delta^{18}O$ and $\delta^{13}C$) were collected from subannually and annually sampled increments along tree-ring chronologies. Mean annual temperatures (MAT) were estimated to be 11.4 °C using $\delta^{18}O$ isotopes, taking the mean of a variety of commonly used mechanistic models (Roden et al., 2000; Anderson et al., 2002) and transfer functions (Ballantyne et al., 2006; Richter et al., 2008b; Csank et al., 2013) designed for estimating temperature with wood cellulose. This value is in agreement with other studies using alternate proxies (Greenwood and Wing, 1995; Sunderlin et al., 2011). The range is 7.5–16.6 °C, which is a 9 °C difference from warmest to coolest MAT. An estimate of $\delta^{13}C$ of Eocene atmosphere (−5.3 ‰) was in agreement with the estimate of Tipple et al. (2010) for ca. 53.3 Ma, who used independent proxy methods (i.e., benthic foraminifera). Seasonal climates were also investigated: mean annual range of temperature was 3.5–16.4 °C ($n = 4$), with a mean of 10.9 °C ($1\sigma = 3.0$ °C). Warm month mean temperatures were $\sim 16.4 \pm 3.0$ °C, but cold month mean temperatures could not be calculated with this

BGD
11, 16269–16308, 2014

archive, as the trees were dormant during winter when continuous darkness persisted. Dual-isotope analysis suggests that a strong interannual (2–3 ypc) signal related to stomatal functioning influenced both isotopes, as they are positively correlated ($\Sigma_{Z\text{-score}}$). However, if the first 4–8 tree rings representing juvenile growth are removed, the dual-isotopes are not correlated, suggesting that factors other than stomatal functioning are more important. Therefore, the most likely explanation for these patterns is that the dominant signal is related to multidecadal climate variability (e.g., Pacific Decadal Oscillation, PDO) responsible for low-frequency shifts in $\delta^{18}O$ of source water, and $\delta^{13}C$ shifts related to cloudiness regimes on bidecadal (20–30 ypc) timescales. The fact that these timescales are similar to a modern day PDO frequency spectrum suggests modern climate dynamics are similar to those experienced during the earliest Eocene, despite pronounced global warmth.

The Supplement related to this article is available online at doi:10.5194/bgd-11-16269-2014-supplement.

Author contributions. B. A. Hook designed study, collected and analyzed data, wrote manuscript, J. Halfar edited manuscript, Z. Gedalof edited manuscript, J. Bollmann edited manuscript, D. Schulze edited manuscript.

Acknowledgements. Funding was provided by J. Halfar at the University of Toronto Mississauga through a National Sciences and Engineering Research Council of Canada Discovery Grant. We thank Ekati Diamond Mine, and Diavik Diamond Mine (jointly owned by Dominion Diamond Corporation and Rio Tinto Group, when Panda Pipe samples were donated, Ekati Diamond Mine was owned by BHP Billiton), for access to sample materials; U. Fekl and U. Wortmann for access to equipment; R.E. Plummer, K.J. Steele and M.N. Evans at the University of Maryland Stable Isotope laboratory for conducting mass spectrometry. J. Basinger for helpful editing suggestions.

BGD
11, 16269–16308, 2014

References

Alton, P. B.: Reduced carbon sequestration in terrestrial ecosystems under overcast skies compared to clear skies, Agr. Forest Meteorol., 148, 1641–1653, 2008.

Anderson, W. T., Bernasconi, S. M., McKenzie, J. A., Saurer, M., and Schweingruber, H. F.: Model evaluation for reconstructing the oxygen isotopic composition in precipitation from tree ring cellulose over the last century, Chem. Geol., 182, 121–137, 2002.

Arens, N. C., Jahren, A. H., and Amundson, R.: Can C3 plants faithfully record the carbon isotopic composition of atmospheric carbon dioxide?, Paleobiology, 26, 137–164, 2000.

Ballantyne, A. P., Rybczynski, N., Baker, P. A., Harington, C. R., and White, D.: Pliocene Arctic temperature contraints from the growth rings and isotopic composition of fossil larch, Palaeogeogr. Palaeocl., 242, 188–200, 2006.

Barbour, M. M., Andrews, T. J., and Farquhar, G. D.: Correlations between oxygen isotope ratios of wood constituents of *Quercus* and *Pinus* samples from around the world, Aust. J. Plant. Physiol., 28, 335–348, 2001.

Barbour, M. M., Walcroft, A. S., and Farquhar, G. D.: Seasonal variation in $\delta^{13}C$ and $\delta^{18}O$ of cellulose from growth rings of *Pinus radiata*, Plant. Cell Environ., 25, 1483–1499, 2002.

Beerling, D. J. and Franks, P. J.: The hidden cost of transpiration, Nature, 464, 495–496, 2010.

Bowen, G. J.: Isoscapes: spatial pattern in isotopic biogeochemistry, Annu. Rev. Earth Pl. Sc., 38, 161–187, 2010.

Bowen, G. J. and Revenaugh, J.: Interpolating the isotopic composition of modern meteoric precipitation, Water Resour. Res., 39, 1299, doi:10.1029/2003WR002086, 2003.

Brendel, O., Ianetta, P. P. M., and Stewart, D.: A rapid and simple method to isolate pure alpha-cellulose, Phytochem. Analysis., 11, 7–10, 2000.

Brinkhuis, H., Schouten, S., Collinson, M. E., Sluijs, A., Sinninghe Damsté, J. S., Dickens, G. R., Huber, M., Cronin, T. M., Onodera, J., Takahashi, K., Bujak, J. P., Stein, R., van der Burgh, J., Eldrett, J. S., Harding, I. C., Lotter, A. F., Sangiorgi, F., van Konijnenburg-van Cittert, H., de Leeuw, J. W., Mattheissen, J., Backman, J., Moran, K., Clemens, S., Eynaud, F., Gattacceca, J., Jakobsson, M., Jordan, R., Kaminski, M., King, J., Koc, N., Martinez, N. C., McInroy, D., Moore, Jr., T. C., O'Regan, M., Pälike, H., Rea, B., Rio, D., Sakamoto, T., Smith, D. C., St John, K. E. K., Suto, I., Suzuki, N., Watanabe, M., and Yamamoto, M.: Episodic fresh surface waters in the Eocene Arctic Ocean, Nature, 441, 606–609, 2006.

BGD
11, 16269–16308, 2014

Brookman, T. and Whittaker T.: Experimental assessment of the purity of α-cellulose produced by variations of the Brendel method: Implications for stable isotope ($\delta^{13}C$, $\delta^{18}O$) dendroclimatology, Geochem. Geophy. Geosy., 13, Q0AI01, doi:10.1029/2012GC004215, 2012.
Bunn, A. G.: A dendrochronology program library in R (dplR), Dendrochronologia, 26, 115–124, 2008.
Bunn, A. G.: Statistical and visual crossdating in R using the dplR library, Dendrochronologia, 28, 251–258, 2010.
Caballero, R. and Huber, M.: Spontaneous transition to superrotation in warm climates simulated by CAM3, Geophys. Res. Lett., 37, L11701, doi:10.1029/2010GL043468, 2010.
Chiacchio, M., Ewen, T., Wild, M., and Arabini, E.: Influence of climate shifts on decadal variations of surface solar radiation in Alaska, J. Geophys. Res., 115, D00D21, doi:10.1029/2009JD012533, 2010.
Creaser, R. A., Grütter, H., Carlson, J., and Crawford, B.: Macrocrystal phlogopite Rb-Sr dates for the Ekati property kimberlites, Slave Province, Canada: evidence for multiple intrusive episodes in the Paleocene and Eocene, Lithos, 76, 399–414, 2004.
Csank, A. Z., Fortier, D., and Leavitt, S. W.: Annually resolved temperature reconstructions from a late Pliocene–early Pleistocene polar forest on Bylot Island, Canada, Palaeogeogr. Palaeocl., 369, 313–322, 2013.
Dansgaard, W.: Stable isotopes in precipitation, Tellus, 16, 368–436, 1964.
Daux, V., Edouard, J. L., Masson-Delmotte, V., Stievenard, M., Hoffmann, G., Pierre, M., Mestre, O., Danis, P. A., and Guibal, F.: Can climate variations be inferred from tree-ring parameters and stable isotopes from *Larix decidua*? Juvenile effects, budmoth outbreaks, and divergence issue, Earth Planet. Sc. Lett., 309, 221–233, 2011.
DeNiro, M. J. and Epstein, S.: Relationship between the oxygen isotope ratios of terrestrial plant cellulose, carbon dioxide, and water, Science, 204, 51–53, 1979.
Eberle, J. J., Fricke, H. C., Humphrey, J. D., Hackett, L., Newbrey, M. G., and Hutchison, J. H.: Seasonal variability in Arctic temperatures during early Eocene time, Earth Planet. Sc. Lett., 296, 481–486, 2010.
Farquhar, G. D., O'Leary, M. H., and Berry, J. A.: On the relationship between carbon isotope discrimination and the intercellular carbon dioxide in leaves, Aust. J. Plant. Physiol., 9, 121–137, 1982.
Farquhar, G. D., Ehleringer, J. R., and Hubick, K. T.: Carbon isotope discrimination and photosynthesis, Annu. Rev. Plant. Phys., 40, 503–537, 1989.

BGD
11, 16269–16308, 2014

Ferrio, J. P. and Voltas, J.: Carbon and oxygen isotope ratios in wood constituents of *Pinus halepensis* as indicators of precipitation, temperature and vapour pressure deficit, Tellus B, 57, 164–173, 2005.

Flanagan, L. B., Comstock, J. P., and Ehleringer, J. R.: Comparison of modeled and observed environmental influences on the stable oxygen and hydrogen isotope composition of leaf water in *Phaseolus vulgaris* L., Plant Physiol., 96, 588–596, 1991.

Francis, J. E.: A 50-million-year-old fossil forest from Strathcona Fiord, Ellesmere Island, Arctic Canada: evidence for a warm polar climate, Arctic, 41, 314–318, 1988.

Francis, J. E. and Poole, I.: Cretaceous and early Tertiary climates of Antarctica: evidence from fossil wood, Palaeogeogr. Palaeocl., 182, 47–64, 2002.

Freeden, A. L. and Sage, R. F.: Temperature and humidity effects on branchlet gas-exchange in white spruce: an explanation for the increase in transpiration with branchlet temperature, Trees, 14, 161–168, 1999.

Fricke, H. C. and O'Neil, J. R.: The correlation between $^{18}O/^{16}O$ ratios of meteoric water and surface temperature: its use in investigating terrestrial climate change over geologic time, Earth Planet. Sc. Lett., 170, 181–196, 1999.

Fricke, H. C. and Wing, S. L.: Oxygen isotope and paleobotanical estimates of temperature and $\delta^{18}O$-latitude gradients over North America during the early Eocene, Am. J. Sci., 304, 612–635, 2004.

Gagen, M., McCarroll, D., Loader, N. J., Robertson, I., Jalkanen, R., and Anchukaitis, K. J.: Exorcising the "segment length curse": summer temperature reconstruction since AD 1640 using non-detrended stable carbon isotope ratios from pine trees in northern Finland, Holocene, 17, 435–446, 2007.

Gaudinski, J. B., Dawson, T. E., Quideau, S., Schuur, E. A. G., Roden, J. S., Trumbore, S. E., Sandquist, D. R., Oh, S.-W., and Wasylishen, R. E.: Comparative analysis of cellulose preparation techniques for use with ^{13}C, ^{14}C, and ^{18}O isotopic measurements, Anal. Chem., 77, 7212–7224, 2005.

Gershunov, A. and Barnett, T. P.: Interdecadal modulation of ENSO teleconnections, B. Am. Meteorol. Soc., 79, 2715–2725, 1998.

Greenwood, D. R. and Wing, S. L.: Eocene continental climates and latitudinal temperature gradients, Geology, 23, 1044–1048, 1995.

Helliker, B. R. and Richter, S. L.: Subtropical to boreal convergence of tree-leaf temperatures, Nature, 454, 511–514, 2008.

BGD
11, 16269–16308, 2014

Hook, B., Halfar, J., Gedalof, Z., and Bollmann, J.: Controlled breaking of mummified wood for use in paleoenvironmental analysis, Tree-Ring Res., 69, 87–92, 2013.
Hook, B., Halfar, J., Bollmann, J., Gedalof, Z., Rahman, M. A., Reyes, J., and Schulze, D.: Comparison of α-cellulose extraction techniques for use with kimberlite-hosted mummified wood, Chem. Geol., in review, 2014.
Huber, M. and Caballero, R.: Eocene El Niño: evidence for robust tropical dynamics in the "hothouse", Science, 299, 877–881, 2003.
Huber, M. and Caballero, R.: The early Eocene equable climate problem revisited, Clim. Past, 7, 603–633, doi:10.5194/cp-7-603-2011, 2011.
Intergovernmental Panel on Climate Change (IPCC): Climate Change 2013: the Physical Science Basis, contribution of Working Group I to the Fifth Assessment Report of the Intergovernmental Panel on Climate Change, edited by: Stocker, T. F., Qin, D., Plattner, G.-K., Tignor, M., Allen, S. K., Boschung, J., Nauels, A., Xia, Y., Bex, V., and Midgley, P. M., Cambridge University Press, Cambridge, UK and New York, NY, USA, 1535 pp., 2013.
Ivany, L. C., Brey, T., Huber, M., Buick, D. P., and Schöne, B. R.: El Niño in the Eocene greenhouse recorded by fossil bivalves and wood from Antarctica, Geophys. Res. Lett., 38, L16709, doi:10.1029/2011GL048635, 2011.
Jahren, A. H. and Sternberg, L. S. L.: Eocene meridional weather patterns reflected in the oxygen isotopes of Arctic fossil wood, GSA Today, 12, 4–9, 2002.
Jahren, A. H. and Sternberg, L. S. L.: Annual patterns within tree rings of the Arctic middle Eocene (ca. 45 Ma): isotopic signatures of precipitation, relative humidity, and deciduousness, Geology, 36, 99–102, 2008.
Jasechko, S., Sharp, Z. D., Gibson, J. J., Birks, J. S., Yi, Y., and Fawcett, P. J.: Terrestrial water fluxes dominated by transpiration, Nature, 496, 347–350, 2013.
Jia, X., Lin, H., and Derome, J.: The influence of tropical Pacific forcing on the Arctic Oscillation, Clim. Dynam., 32, 495–509, 2009.
Johnstone, J. A., Roden, J. S., and Dawson, T. E.: Oxygen and carbon stable isotopes in coast redwood tree rings respond to spring and summer climate signals, J. Geophys. Res.-Biogeo., 118, 1438–1450, 2013.
Laskar, J., Fienga, A., Gastineau, M., and Manche, H.: La2010: a new orbital solution for the long term motion of the Earth, La2010 v4, Astron. Astrophys., 532, A89, doi:10.1051/0004-6361/201116836, 2011.

BGD
11, 16269–16308, 2014

Libby, L. M. and Pandolfi, L. J.: Temperature dependence of isotope ratios in tree rings, P. Natl. Acad. Sci. USA, 71, 2482–2486, 1974.
Libby, L. M., Pandolfi, L. J., Payton, P. H., Marshall III, J., Becker, B., and Giertz-Sienbenlist, V.: Isotopic tree thermometers, Nature, 261, 284–288, 1976.
Liu, X., Shao, X., Liang, E., Zhao, L., Chen, T., Qin, D., and Ren, J.: Species-dependent responses of juniper and spruce to increasing CO_2 concentration and to climate in semi-arid and arid areas of northwestern China, Plant. Ecol., 193, 195–209, 2007.
Liu, X., An, W., Leavitt, S. W., Wang, W., Xu, G., Zeng, X., and Qin, D.: Recent strengthening of correlations between tree-ring $\delta^{13}C$ and $\delta^{18}O$ in mesic western China: implications to climatic reconstruction and physiological responses, Global Planet. Change, 113, 23–33, 2014.
Lomax, B. H., Knight, C. A., and Lake, J. A.: An experimental evaluation of the use of $C_3\delta^{13}C$ plant tissue as a proxy for the paleoatmospheric $\delta^{13}CO_2$ signature of air, Geochem. Geophy. Geosy., 13, Q0AI03, doi:10.1029/2012GC004174, 2012.
Majoube, M.: Fractionement en oxygéne-18 et en deutérium entre l'eau et sa vapeur, J. Chem. Phys., 197, 1423–1426, 1971.
Mann, M. and Lees, J.: Robust estimation of background noise and signal detection in climatic time series, Clim. Change, 33, 409–335, 1996.
Mantua, N. J., Hare, S. R., Zhang, Y., Wallace, J. M., and Francis, R. C.: A Pacific interdecadal climate oscillation with impacts on salmon production, B. Am. Meteorol. Soc., 78, 1069–1079, 1997.
McCarroll, D. and Loader, N. J.: Stable isotopes in tree rings, Quaternary Sci. Rev., 23, 771–801, 2004.
McCarroll, D., Gagen, M. H., Loader, N. J., Robertson, I., Anchukaitis, K., Los, S., Young, G. H. F., Jalkanen, R., Kirchhefer, A., and Waterhouse, J. S.: Correction of tree ring stable carbon isotope chronologies for changes in carbon dioxide content of the atmosphere, Geochim. Cosmochim. Ac., 73, 1539–1547, 2009.
Reinhardt, K., Smith, W. K., and Carter, G. A.: Clouds and cloud immersion alter photosynthetic light quality in a temperate mountain cloud forest, Botany, 88, 462–470, 2010.
Richter, S. L., Johnson, A. H., Dranoff, M. M., LePage, B. A., and Williams, C. J.: Oxygen isotope ratios in fossil wood cellulose: isotopic composition of Eocene- to Holocene-aged cellulose, Geochim. Cosmochim. Ac., 72, 2744–2753, 2008a.

BGD
11, 16269–16308, 2014

Richter, S. L., Johnson, A. H., Dranoff, M. M., and Taylor, K. D.: Continental-scale patterns in modern wood cellulose δ^{18}O: implications for interpreting paleo-wood cellulose δ^{18}O, Geochim. Cosmochim. Ac., 72, 2735–2743, 2008b.

Ritchie, R. J.: Modelling photosynthetic photon flux density and maximum potential gross photosynthesis, Photosynthetica, 48, 596–609, 2010.

Roden, J. S. and Farquhar, G. D.: A controlled test of the dual-isotope approach for the interpretation of stable carbon and oxygen isotope ratio variation in tree rings, Tree Physiol., 32, 490–503, 2012.

Roden, J. S., Lin, G., and Ehleringer, J. R.: A mechanistic model for interpretation of hydrogen and oxygen ratios in tree-ring cellulose, Geochim. Cosmochim. Ac., 64, 21–35, 2000.

Roden, J. S., Johnstone, J. A., and Dawson, T. E.: Intra-annual variation in the stable oxygen and carbon isotope ratios of cellulose in tree rings of coast redwood (*Sequoia sempervirens*), Holocene, 19, 189–197, 2009.

Royer, D. L.: CO_2-forced climate thresholds during the Phanerozoic, Geochim. Cosmochim. Ac., 70, 5665–5675, 2006.

Saurer, M., Siegenthaler, U., and Schweingruber, H. F.: The climate-carbon isotope relationship in tree rings and the significance of site conditions, Tellus B, 47, 320–330, 1995.

Saurer, M., Aellen, K., and Siegwolf, R.: Correlating δ^{13}C and δ^{18}O in cellulose of trees, Plant. Cell Environ., 20, 1543–1550, 1997.

Scheidegger, Y., Saurer, M., Bahn, M., and Siegwolf, R.: Linking stable oxygen and carbon isotopes with stomatal conductance and photosynthetic capacity: a conceptual model, Oecologia, 125, 350–357, 2000.

Schubert, B. A. and Jahren, A. H.: Reconciliation of marine and terrestrial carbon isotope excursions based on changing atmospheric CO_2 levels, Nat. Commun., 4, 1–6, 2013.

Sewall, J. O. and Sloan, L. C.: Equable Paleogene climates: the result of a stable, positive Arctic Oscillation?, Geophys. Res. Lett., 28, 3693–3695, 2001.

Simard, S., Morin, H., Krause, C., Buhay, W. M., and Treydte, K.: Tree-ring widths and isotopes of artificially defoliated balsam firs: a simulation of spruce budworm outbreaks in Eastern Canada, Environ. Exp. Bot., 81, 44–54, 2012.

Stokes, M. A. and Smiley, T. L.: An Introduction to Tree-Ring Dating, Univ. of Chicago Press, Chicago, IL, 73 pp., 1968.

BGD
11, 16269–16308, 2014

Sunderlin, D., Loope, G., Parker, N. E., and Williams, C. J.: Paleoclimatic and paleoecological implications of a Paleocene–Eocene fossil leaf assemblage, Chickaloon Formation, Alaska, Palaios, 26, 335–345, 2011.

Tipple, B. J., Meyers, S. R., and Pagani, M.: Carbon isotope ratio of Cenozoic CO_2: a comparative evaluation of available geochemical proxies, Paleoceanography, 25, PA3202, doi:10.1029/2009PA001851, 2010.

Urban, O., Klem, K., Ač, A., Havránková, K., Holišová, P., Navrátil, M., Zitová, M., Kozlová, K., Pokorný, R., Šprtová, M., Tomášková, I., Špunda, V., and Grace, J.: Impact of clear and cloudy sky conditions on the vertical distribution of photosynthetic CO_2 uptake within a spruce canopy, Funct. Ecol., 26, 46–55, 2012.

Vautard, R. and Ghil, M.: Singular spectrum analysis in nonlinear dynamics, with applications to paleoclimatic time series, Physica D, 32, 395–424, 1989.

Vowinckel, T., Oechel, W. C., and Boll, W. G.: The effect of climate on the photosynthesis of Picea mariana at the subarctic tree line. 1. Field measurements, Can. J. Bot., 53, 604–620, 1975.

Wallin, G. and Skärby, L.: The influence of ozone on the stomatal and non-stomatal limitation of photosynthesis in Norway spruce, *Picea abies* (L.) Karst, exposed to soil moisture deficit, Trees, 6, 128–136, 1992.

Weijers, J. W. H., Schouten, S., Sluijs, A., Brinkhaus, H., and Sinninghe Damsté, J. S.: Warm arctic continents during the Palaeocene–Eocene thermal maximum, Earth Planet. Sc. Lett., 261, 230–238, 2007.

Werner, R. A., Kornexl, B. E., Roßmann, A., and Schmidt, H. L.: On-line determination of δ^{18}O-values of organic substances, Anal. Chim. Acta, 319, 159–164, 1996.

Williams, C. J., Johnson, A. H., LePage, B. A., Vann, D. R., and Sweda, T.: Reconstruction of Tertiary *Metasequoia* forests. II. Structure, biomass, and productivity of Eocene floodplain forests in the Canadian Arctic, Paleobiology, 29, 271–292, 2003.

Wolfe, A. P., Csank, A. Z., Reyes, A. V., McKellar, R. C., Tappert, R., and Muehlenbachs, K.: Pristine early Eocene wood buried deeply in kimberlite from northern Canada, PLoS ONE, 7, e45537, doi:10.1371/journal.pone.0045537, 2012.

Young, G. H. F., McCarroll, D., Loader, N. J., Gagen, M. H., Kirchhefer, A. J., and Demmler, J. C.: Changes in atmospheric circulation and the Arctic Oscillation preserved within a millennial length reconstruction of summer cloud cover from northern Fennoscandia, Clim. Dynam., 39, 495–507, 2012.

BGD
11, 16269–16308, 2014

Young, G. H. F., McCarroll, D., Loader, N. J., and Kirchhefer, A. J.: A 500 year record of summer near-ground solar radiation from tree-ring stable carbon isotopes, Holocene, 20, 315–324, 2010.

Zachos, J., Pagani, M., Sloan, L., Thomas, E., and Billups, K.: Trends, rhythms, and aberrations in global climate 65 Ma to present, Science, 292, 686–693, 2001.

BGD
11, 16269–16308, 2014

Table 1. Summary of equations used in oxygen isotope temperature reconstruction. Mechanistic models and transfer functions used to predict $\delta^{18}O_{sw}$ from $\delta^{18}O_{cellulose}$, and a temperature–$\delta^{18}O_{sw}$ relationship developed for the Eocene (Fricke and Wing, 2004). Shown are each equation and the reference on which it is based.

Type of analysis	Used to calculate	Reference
Mechanistic models		
$\delta^{18}O_{wl} = \{(\alpha[\alpha_k \cdot R_{wx}(e_i - e_a/e_i) + R_{wa}(e_a/e_i)]/0.0020052) - 1\} \cdot 1000$	$\delta^{18}O_{wl}$	Flanagan et al. (1991)
$\delta^{18}O_{cellulose} = f_O \cdot (\delta^{18}O_{wx} + \varepsilon_O) + (1 - f_O) \cdot (\delta^{18}O_{wl} + \varepsilon_O)$	$\delta^{18}O_{wx}$	Roden et al. (2000)[a]
$\delta^{18}O_{sw} \approx \delta^{18}O_{cellulose} - (1 - f) \cdot (1 - h) + (\alpha + \alpha_k) - \varepsilon_{biochem}$	$\delta^{18}O_{sw}$	Anderson et al. (2002)
Transfer functions		
$\delta^{18}O_{sw} = 312.75 \cdot e^{(-0.13 \cdot \delta^{18}O_{cellulose})}$	$\delta^{18}O_{sw}$	Ballantyne et al. (2006)
$\delta^{18}O_{sw} = (\delta^{18}O_{cellulose} - 35.11)/0.59$	$\delta^{18}O_{sw}$	Richter et al. (2008b)[b]
$\delta^{18}O_{sw} = (\delta^{18}O_{cellulose} - 33.2045)/0.6109$	$\delta^{18}O_{sw}$	Csank et al. (2013)[b]
$\delta^{18}O_{sw} = -0.017^2 + T - 22.91$	T (°C)	Fricke and Wing (2004)[c]

[a] Equation solved for $\delta^{18}O_{wx}$, which is used as a surrogate for $\delta^{18}O_{sw}$.
[b] Linear transfer functions estimating $\delta^{18}O_{cellulose}$ were solved for $\delta^{18}O_{sw}$ as shown here.
[c] A fourth-order polynomial, based on the Fricke and Wing (2004) polynomial shown here, was used to estimate T (°C) based on the different $\delta^{18}O_{sw}$ estimates from mechanistic models and transfer functions: T (°C) = $(0.000005 \cdot \delta^{18}O_{sw}^4) + (0.0007 \cdot \delta^{18}O_{sw}^3) + (0.0436 \cdot \delta^{18}O_{sw}^2) + (2.1153 \cdot \delta^{18}O_{sw}) + 32.697$.

BGD
11, 16269–16308, 2014

Table 2. Early Eocene Mean Annual Temperature (MAT) estimates based on $\delta^{18}O$ of Piceoxylon cellulose. Several methods of temperature estimation in the literature were used, including mechanistic models (Roden et al., 2000; Anderson et al., 2002) and transfer functions (Csank et al., 2013; Richter et al., 2008b; Ballantyne et al., 2006) that predict $\delta^{18}O_{sw}$ from $\delta^{18}O_{cellulose}$. MAT was derived from $\delta^{18}O_{sw}$ using a $\delta^{18}O_{sw}$–temperature relationship developed for the Eocene (Fricke and Wing, 2004). Shown are references for model/function, relative humidity level (for mechanistic models), range (min–max) of MAT (°C), and mean (SD) of MAT (°C) in chronology.

Reference	Relative Humidity	Range MAT (°C)	Mean (sd) MAT (°C)
Mechanistic Models			
Roden et al. (2000)	64 %	1–12.6	5.9 (2.3)
	77 %	4.6–17.4	10.0 (2.6)
	83 %	6.1–19.5	11.7 (2.7)
Anderson et al. (2002)	64 %	10.6–16.3	13.1 (1.2)
	77 %	13.3–19.5	16.0 (1.3)
	83 %	15.3–21.9	18.2 (1.3)
Transfer Functions			
Csank et al. (2013)		6.5–15.4	10.3 (1.8)
Richter et al. (2008b)		2.4–10.5	5.9 (1.7)
Ballantyne et al. (2006)		7.7–16.4	11.9 (1.8)
Mean of all methods		7.5–16.6	11.4 (1.8)

BGD
11, 16269–16308, 2014

Table 3. Range of possible $\delta^{13}C_{atm}$ and Δ at different c_i/c_a levels, given a mean $\delta^{13}C_{cellulose}$ of −20.8 ‰. Shown are various c_i/c_a values, Δ values, $\delta^{13}C_{atm}$ (‰) values based on the average $\delta^{13}C$ of tree-ring cellulose from this study, $\delta^{13}C_{atm}$ (‰) values based on benthic foraminifera (Tipple et al., 2010), and bounds of the values in previous column.

This Study			Tipple et al. (2010)	
c_i/c_a	Δ	$\delta^{13}C_{atm}$ (‰)	$\delta^{13}C_{atm}$ (‰)	$\delta^{13}C_{atm}$ (‰) bounds
0.6	17.96	−6.3	−6.3	upper 90 %
0.63	18.64	−5.6	−5.7	mean
0.66	19.32	−5.0	−4.8	lower 90 %

BGD
11, 16269–16308, 2014

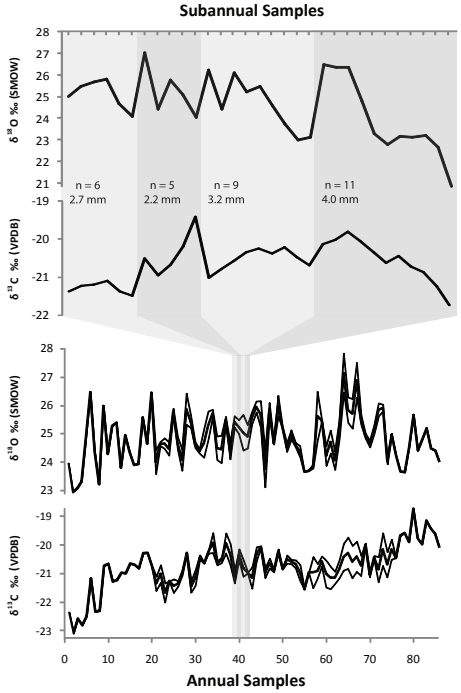

Figure 1. Subannual and annual-resolution records of tree-ring cellulose $\delta^{18}O$ and $\delta^{13}C$. Shaded bars show the four tree rings sampled subannually (TR 39–42), number of slices per tree ring (n) and ring width (mm) are shown in each bar between the upper two lines depicting seasonal $\delta^{18}O$ and $\delta^{13}C$ data. Bold lines in the lower two graphs show mean isotope values of annual-resolution study, thin lines show minimum and maximum isotope values of crossdated tree-ring transects (TR 21–54, 57–75).

BGD
11, 16269–16308, 2014

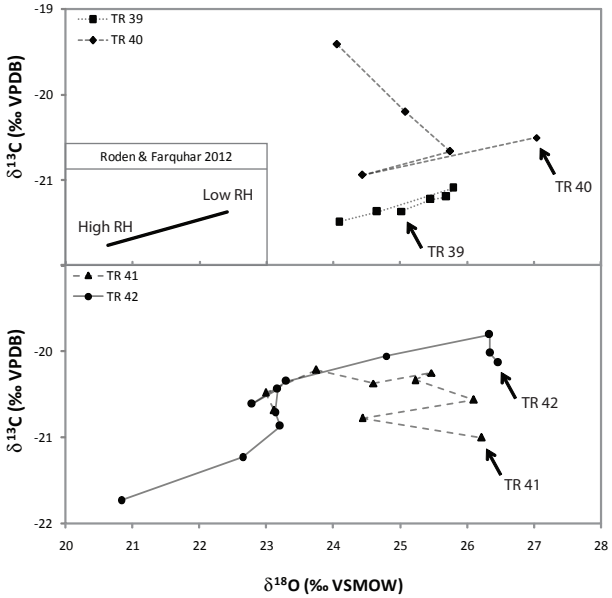

Figure 2. Scatterplots of dual-isotope data for four tree rings (TR 39–42), showing trends of $\delta^{18}O$ and $\delta^{13}C$ within a growing season. Arrows point to the start of each numbered tree ring (earlywood), lines connect to consecutive samples (latewood) within each tree ring. Upper graph contains first two tree rings, and lower graph the third and fourth rings. Inset box in upper graph shows average low to high RH for *Pinus radiata* D. Don (after Roden and Farquhar, 2012). Low-to-high RH dual-isotope relationship: [$\delta^{13}C = 0.22 \cdot \delta^{18}O - 31.31$]. Scale is the same for inset graph, but actual values of Roden and Farquhar, 2012 ($\delta^{18}O$ low RH = 29.26 ‰, $\delta^{18}O$ high RH = 26.9 ‰ ; $\delta^{13}C$ low RH = −24.86 ‰, $\delta^{18}O$ high RH = −25.38 ‰) do not correspond with these axes.

BGD
11, 16269–16308, 2014

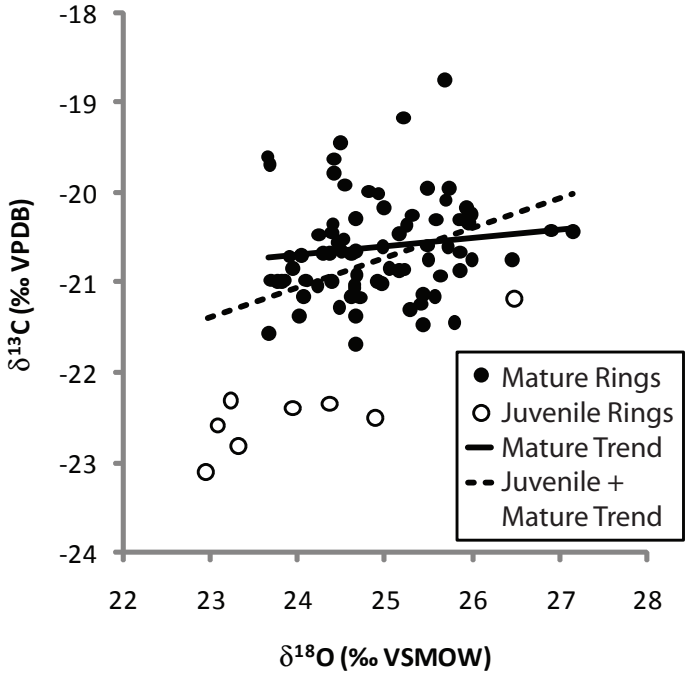

Figure 3. Correlation analysis of dual-isotope annual dataset. $\delta^{18}O$ and $\delta^{13}C$ were significantly positively correlated (dashed trendline; Pearson's $R = 0.36$, $P < 0.001$, $n = 86$). However, if the first 4–8 "juvenile" tree rings (hollow circles) are removed from analysis, the remaining samples (filled circles) are not correlated (solid trendline; Pearson's $R = 0.14$, $P = 0.22$, $n = 78$).

BGD
11, 16269–16308, 2014

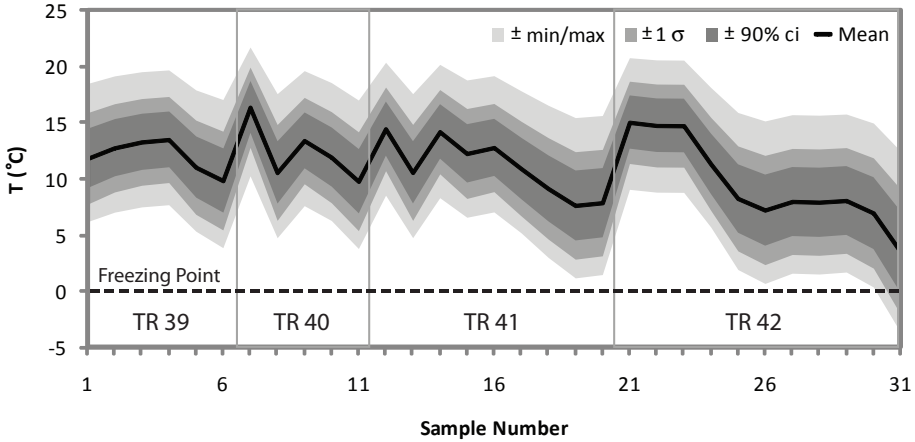

Figure 4. Mean temperature (˚C) of subannual data based on all δ^{18}O-temperature reconstructions. Mean of all reconstructions (black line) is bracketed by 90 % confidence interval (±90 % ci, dark gray fill), one SD (±1 σ, medium gray fill), and minimum/maximum (± min/max, light gray fill). Freezing point is shown by dashed line.

BGD
11, 16269–16308, 2014

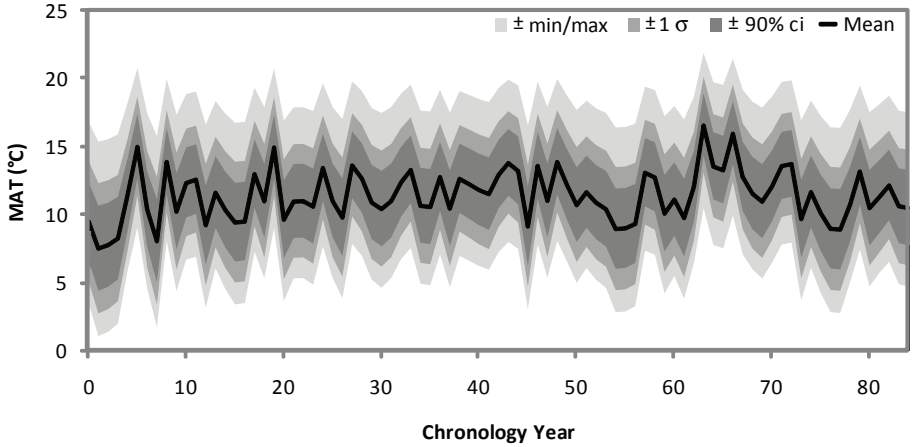

Figure 5. Mean annual temperature (MAT °C) based on all δ^{18}O-temperature reconstructions. Mean of all reconstructions (black line) is bracketed by 90 % confidence interval (±90 % ci, dark gray fill), one SD (±1 σ, medium gray fill), and minimum/maximum (± min/max, light gray fill) estimates.

BGD
11, 16269–16308, 2014

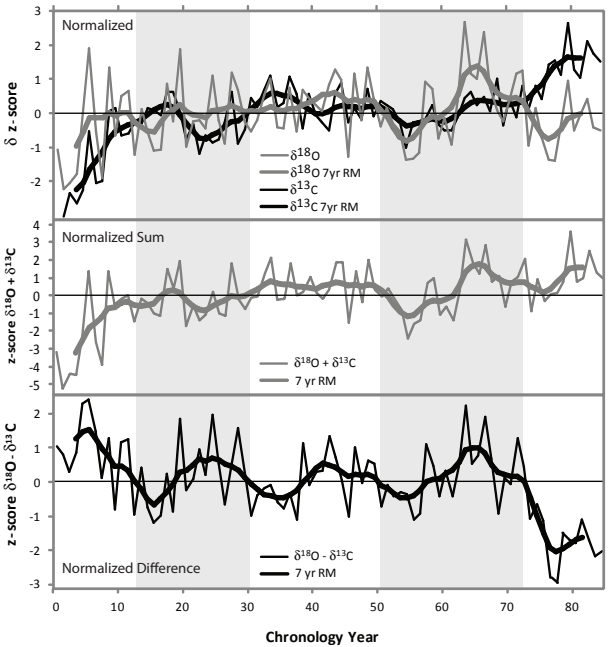

Figure 6. Results of dual-isotope (δ^{18}O and δ^{13}C) analysis (ISO chronology, $n = 86$). Upper panel: Normalized δ^{18}O ($\delta^{18}O_{Z\text{-score}}$, thin gray line) and δ^{13}C ($\delta^{13}C_{Z\text{-score}}$ thin black line), and 7 year triangular running mean $\delta^{18}O_{Z\text{-score}}$ (bold gray line) and $\delta^{13}C_{Z\text{-score}}$ (bold black line). Center panel: Sum of $\delta^{18}O_{Z\text{-score}}$ and $\delta^{13}C_{Z\text{-score}} = \Sigma_{Z\text{-score}}$ (thin gray line), and 7 year triangular running mean (bold gray line). Lower panel: Difference of $\delta^{18}O_{Z\text{-score}}$ minus $\delta^{13}C_{Z\text{-score}} = \Delta_{Z\text{-score}}$ (thin black line), and 7 year triangular running mean (bold black line). Shaded regions in upper and lower panels highlight the bidecadal oscillations especially evident in the PC2 ($\Delta_{Z\text{-score}}$) chronology in the lower panel.

BGD
11, 16269–16308, 2014

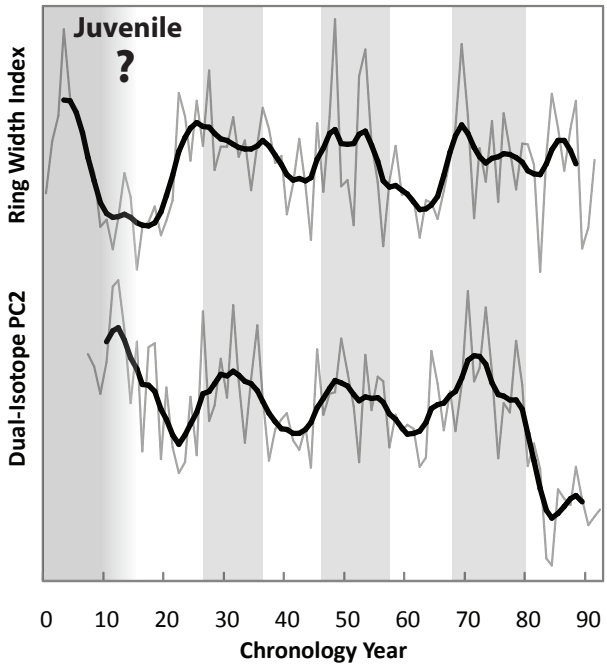

Figure 7. Correspondence of *Piceoxylon* tree-ring width indices (RWI) and stable isotope chronologies. (*Upper*) *Piceoxylon* RWI ($n = 92$, gray line) with 7 year triangular running mean (bold black line) to highlight low-frequency variability. (*Lower*) *Piceoxylon* isotope PC2 chronology ($n = 86$, gray line) with 7 year triangular running mean (bold black line) to highlight low-frequency variability. Here, grey boxes denote warmer and cloudier decades with above average tree ring growth. The first seven tree rings of the RWI record were not analyzed for stable isotopes, due to concerns about possible influences of juvenile tree growth on the isotope record. Question mark at the beginning of the RWI record depicts uncertainty due to a possible juvenile growth signal.

BGD
11, 16269–16308, 2014

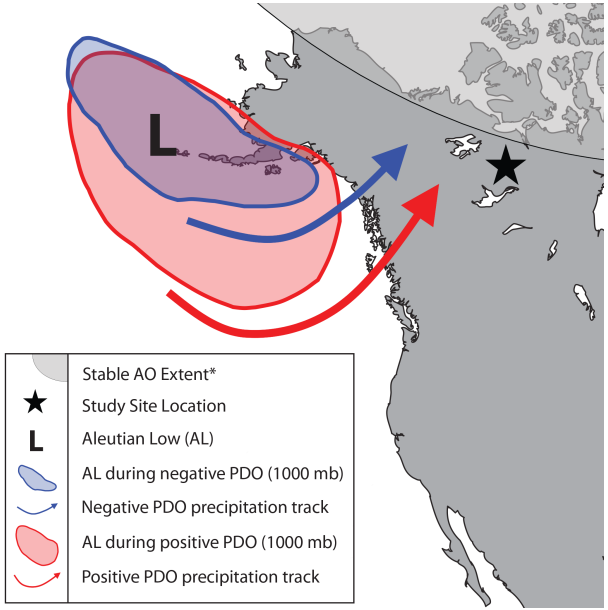

Figure 8. Position and strength of Aleutian low-pressure system during positive and negative phases of the PDO in relation to study site. Hypothesized stable Arctic Oscillation during the Eocene depicted by grey arc in upper right corner (*see Sewall and Sloan, 2001). 1000 mb sea level pressure (SLP) contours shown for negative PDO (blue shaded area) and positive PDO (red shaded area). Weather patterns are altered according to these changes in SLP (blue arrow – negative PDO, red arrow – positive PDO), thus altering the distribution of precipitation across North America. Positions of 1000 mb contours of Aleutian low after NOAA-CIRES/Climate Diagnostics Center (January–March sea level pressure (mb) composite for negative PDO 1988, 1999; for positive PDO 1983, 1987, 1992, 1998).

BGD
11, 16269–16308, 2014